Supporting Information for Synthesis and Electronic Structure of a 3D Crystalline Stack of MXene-Like Sheets

Daniel L. Druffel,[†] Matthew G. Lanetti,[†] Jack D. Sundberg,[†] Jacob T. Pawlik,[†] Madeline S. Stark,[†] Carrie L. Donley,[‡] Lauren M. McRae,[†] Katie M. Scott,[†] and Scott C. Warren[*,†,¶]

†*Department of Chemistry, University of North Carolina at Chapel Hill, Chapel Hill, North Carolina 27599, United States*

‡*Chapel Hill Analytical and Nanofabrication Laboratory (CHANL), University of North Carolina at Chapel Hill, Chapel Hill, North Carolina, 27599, United States*

¶*Department of Applied Physical Sciences, University of North Carolina at Chapel Hill, Chapel Hill, North Carolina 27599, United States*

E-mail: sw@unc.edu

Additional details about the synthesis of Y_2CF_2

The tantalum ampoule was welded inside of a Centorr arc-melter with a custom-built adapter to hold the ampoule while welding. We ran the reaction at 1240 °C for two reasons: first, we recognized that Y metal, graphite, and YF_3 all have high melting points (1526, ∼4800, and 1387 °C respectively).[1–3] Therefore, the reaction is likely a solid-state reaction with the kinetics governed by diffusion of atoms through the solids. Higher temperatures, like 1240 °C, greatly accelerate the kinetics of solid-state reactions. Secondly, this temperature is at

the highest end of temperatures where fused quartz maintains its mechanical strength. We use sealed quartz jackets to prevent oxidation of the tantalum ampoules at high temperature. In our experiments, lower reaction temperatures (1100 °C) yielded poor products with significant amounts of unreacted reagents. The reaction at 1240 °C yields beautiful reflective green crystals, typically tens to hundreds of μm in size. We did not attempt reactions for shorter times than 3 days, as the syntheses of related carbide halides (e.g. Sc_2CCl_2 and Y_2CCl_2) were conducted for 3–5 days.[4]

X-ray diffraction experiments of Y_2CF_2

We performed X-ray diffraction measurements in two geometries, either a transmission capillary geometry (Fig 1, S8) or a Bragg-Brentano geometry (Fig S1, S2, S13). The measurements in the transmission capillary geometry were used for refinement while those in the Bragg-Brentano geometry were used for quick phase identification. The apparent difference in signal-to-noise between the two geometries is due to the amount of sample irradiated and the collection time. Capillary transmission measurements require longer collection times to acquire quality data.

To show unambiguously that Y_2CF_2 is truly a 2D stacked structure, we performed a measurement in the Bragg-Brentano geometry beginning at an angle of 10° (Figure S1). This diffraction pattern captures the $\{00l\}$ set of planes, including the reflection from the (001) plane at 14.05° and the (002) plane at 28.32°, which nearly overlaps with the reflection of the (100) plane (Figure S1b).

We loaded powders into 7 μm diameter Borosilicate capillaries in the glovebox to perform a measurement in the transmission geometery. We performed a θ-θ measurement at a slow speed of 0.25°/min and rotated the capillary to ensure good counting statistics and obtain a high-quality diffraction pattern. These diffraction patterns are dominated by the peaks from Y_2CF_2 and could be easily indexed and refined. The patterns also reveal the presence of a

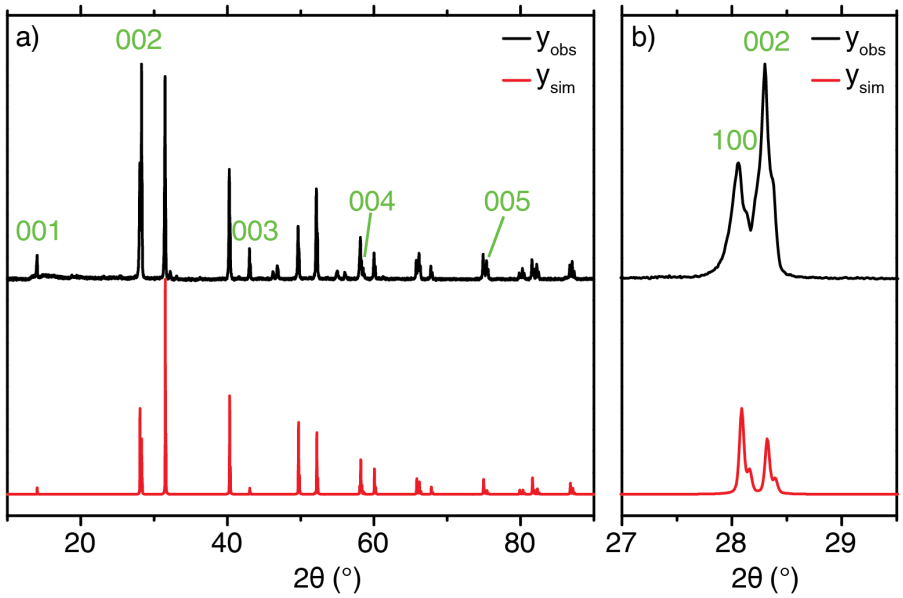

Figure S1: Powder X-ray diffraction pattern of Y_2CF_2 collected using the Bragg-Brentano reflection geometry at low angles to show the reflections from the $\{00l\}$ set of planes, which are labeled in green. The sample was loaded under onto a flat glass substrate and sealed beneath Kapton tape. The data is compared to a diffraction pattern simulated using the refined crystal structure of Y_2CF_2 and the Materials Studio software. The simulated data deliberately does not consider preferred orientation to highlight that the intensities of the peaks from the $\{00l\}$ set of planes in the experimental data are increased by strong preferred orientation. b) A zoom in on the data at 28° to show that the (002) plane at 28.32° does not overlap with the reflection of the (100) plane at 28.09°.

minor impurity phase, which could be indexed to a yttrium oxide fluoride. Because many phases of yttrium oxide fluorides share very related crystal structures, the exact phase could not be identified at such a low fraction of the sample. The sample could be α-YOF, $Y_5O_4F_7$, or $Y_6O_5F_8$. In any case, the presence of the phase by weight is less than 5% by mol and in some samples as little as 1% by mol. While this impurity does complicate the analysis of the stoichiometry, it does not impede our analysis of the structure or properties.

We believe that the oxygen in the impurity phase originates from oxygen already present in the yttrium metal reactant when purchased for a few reasons: 1) powdered yttrium metal is notoriously difficult to purify of oxygen and in our experience almost always contains oxygen up to 1-5% by wt; 2) we attempted reactions with added Zr-foil to scavenge oxygen and this did not change the concentration of the impurity phase. For this reason, we attempted to

synthesize an alternative source of yttrium, reacting dendritic Y, which has far less oxygen than powdered sources, with carbon to form a brittle yttrium-carbide phase, which we could mill into a powder. We attempted reacting this yttrium carbide with additional graphite and yttrium fluoride in the following reaction:

$$2Y_2C + C + 2YF_3 \rightarrow 3Y_2CF_2 \tag{1}$$

This reaction also yielded beautiful green crystals of Y_2CF_2 (Figure S2), but the X-ray diffraction measurements still reveal the presence of a yttrium oxide fluoride (Figure S2). It is possible that the yttrium carbide reacted with a small amount of oxygen during synthesis and handling or that the oxygen comes from the yttrium fluoride that we purchased.

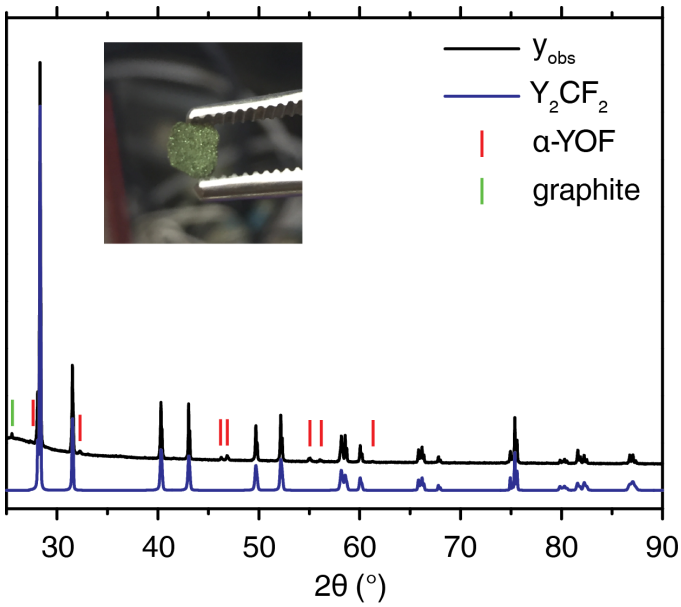

Figure S2: Powder X-ray diffraction pattern of Y_2CF_2 synthesized from Y_2C as described in equation 1. The sample was loaded under onto a flat glass substrate and sealed beneath Kapton tape. The data was colected using the Bragg-Brentano reflection geometry. The intensities of the peak $\sim 28°$ is increased by strong preferred orientation.

Microscopy and spectroscopy of Y_2CF_2

During these experiments, the samples were briefly exposed to air. In the case of the SEM (Figure S3, S4, S7), samples were loaded onto the stage in the glovebox, sealed in plastic, and brought to the instrument. The total exposure to air was less than 5 seconds. The optical microscopy and reflection spectroscopy (Figure S5) was performed in air within the span of one hour. No changes in the material were apparent during that time. For the transmission measurements (Figure S6), the discs were encased within glass wells and and sealed between two pieces of optical-grade quartz using a two-part epoxy inside of the glovebox.

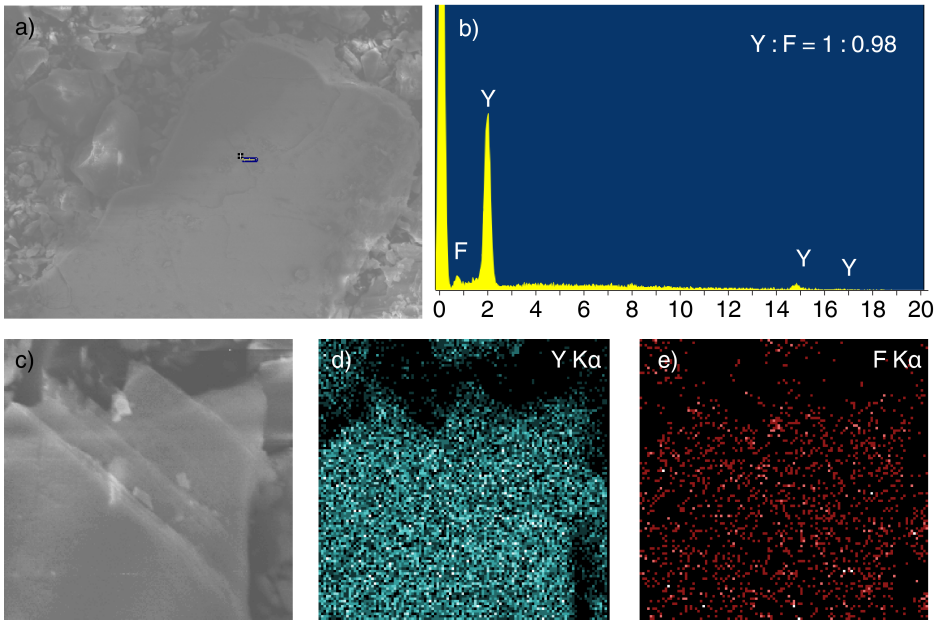

Figure S3: a) Scanning electron image of a Y_2CF_2 surface corresponding to an b) energy dispersive X-ray spectroscopy (EDS) spectrum, which reveals the ratio of Y:F is 1:0.98 $\pm$ 0.05. c) Another scanning electron image of a flaky crystal of Y_2CF_2 and corresponding EDS maps, which reveal that yttrium and fluorine are homogenous throughout the crystal and spatially correlated, as expected.

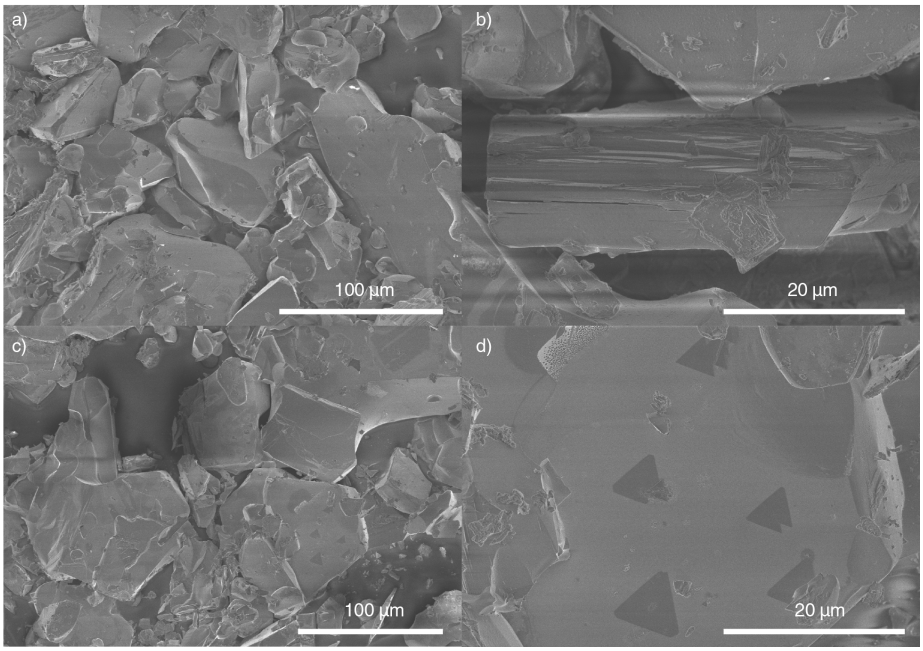

Figure S4: Scanning electron images showing a,c) the faceted morphology of Y_2CF_2 only lightly ground in a mortar and pestle, b) the layered crystal morphology, and d) triangular growth pits aligned on the surface of a crystal that highlight the crystalline and hexagonal structure of Y_2CF_2.

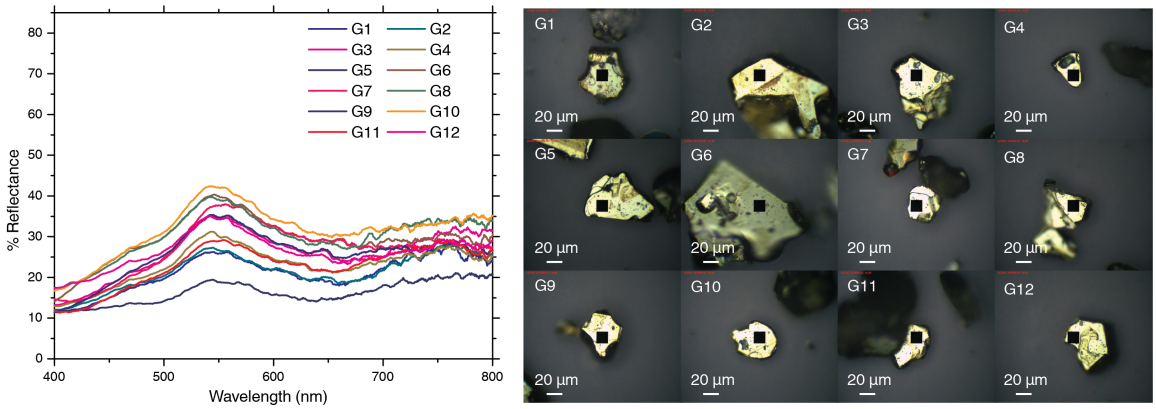

Figure S5: Spectra collected from clean facets of Y_2CF_2 in a microspectrophotometer and their corresponding images.

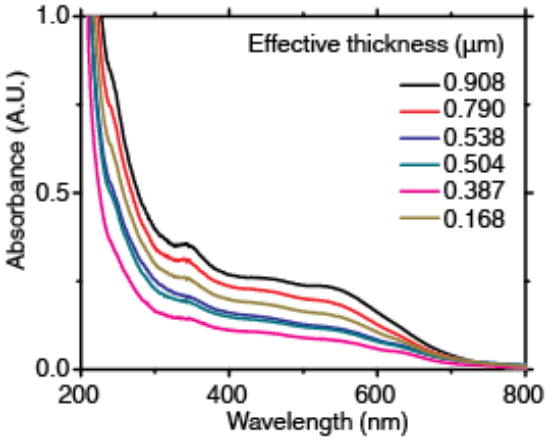

Figure S6: Absorbance spectra of Y_2CF_2. The Y_2CF_2 powder was ground very finely and diluted with spectroscopic grade KBr. The mixture was ground until homogenous, then pressed into discs using the pellet press. The thickness of the discs was approximately 1 mm. The background due to scattering from KBr was subtracted by pressing a number of films of KBr of varying thickness to estimate its effective attenuation as a function of thickness and subtracting a weighted fraction from the acquired spectra. Some films had to be re-run and others re-made to avoid specks of inhomogeneity. All discs appeared red, not green. The spectra were collected by measuring the transmission of light through the thin discs.

Ball milled samples of Y_2CF_2

For some experiments, samples were ball-milled for 15 minutes to reduce the particle size. After ball-milling, the particles were smaller than 5 μm in diameter (Figure S7). We performed powder X-ray diffraction in a transmission capillary geometry, which afforded a pattern (Figure S8) nearly identical to that of the un-milled sample. This confirmed that ball-milling for 15 minutes has no effect on the crystal structure. We performed reflectance measurements on the ball-milled powder (Figure S9) and found that the reflectance peak at 540 nm for faceted Y_2CF_2 particles is not present.

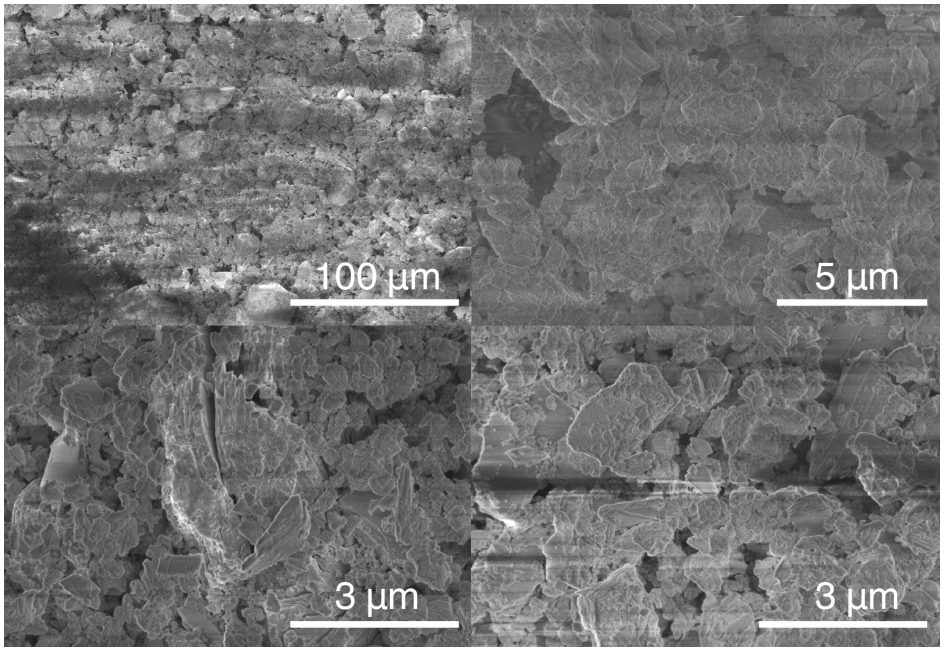

Figure S7: Micrographs of Y_2CF_2 ball-milled to < 5 μm particles.

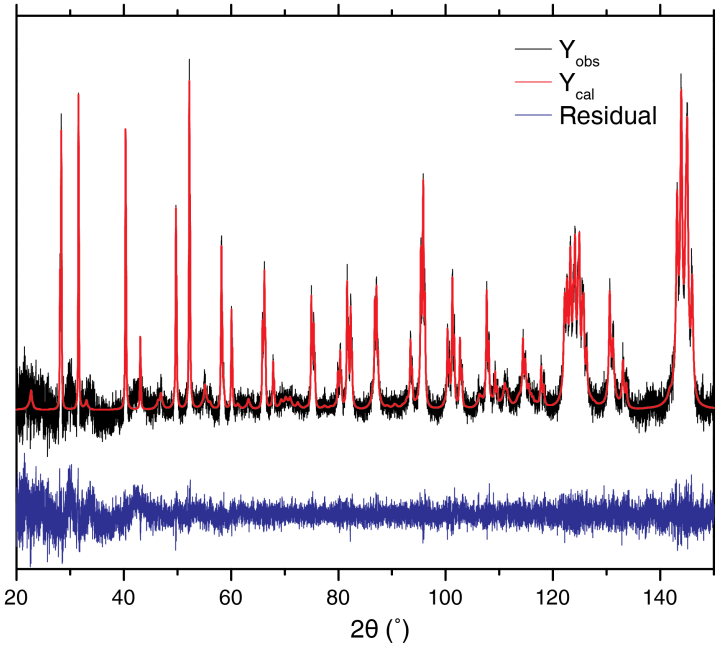

Figure S8: Powder X-ray diffraction pattern of Y_2CF_2 ball milled for 15 minutes, acquired using a Rigaku Smartlab diffractometer with a Cu Kα source. The red powder was loaded into a capillary tube and measured using the transmission reflection geometry. The crystal structure, including the lattice constants, remain unchanged through the milling process. As in the un-milled sample, a minor impurity phases, α-YOF, was detected.

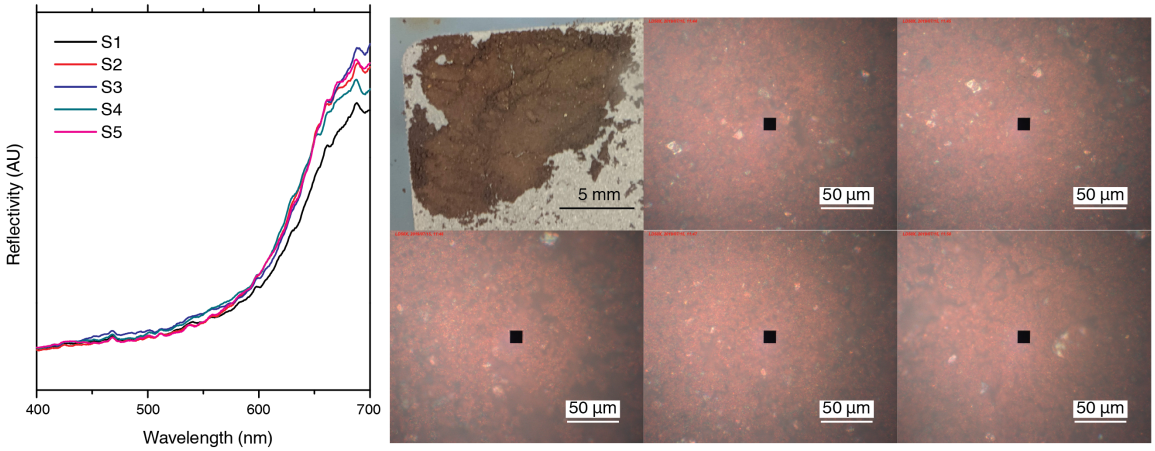

Figure S9: Reflectivity of ball-milled Y_2CF_2, which has no peak at 540 nm. Instead the reflectivity decreases at higher energy wavelengths as a fraction of that light is absorbed by the sample. The red powder is shown in the images on the right.

Oxidation of Y_2CF_2

We studied to oxidation of Y_2CF_2 in air simply by letting the sample sit in an open, uncapped scintillation vial for extended periods of time (e.g. 1 week or 1 month). After 1 week, the once-green sample appears red (Figure S10). We performed reflectance measurements on the air-exposed samples and observe rainbow-like coloration and oscillations in the reflection spectra (Figure S11). We attribute these features to thin-film effects, which alter the reflection at the surface. We performed XPS measurements of the air-exposed samples and found evidence of a carbonate species. We attempted to clean the surface by sputtering the sample with Ar-ions for 15 minutes inside of the XPS instrument. The peaks broadening considerably after sputtering (Figure S12). Peak broadening after Ar-ion sputtering has been observed for other MXenes as well.[5,6] We performed an X-ray diffraction measurement in a Bragg-Brentano geometry after exposing Y_2CF_2 powder to air for 3 weeks (Figure S13). The diffraction pattern reveals that, a crystalline yttrium oxide fluoride develops slowly over time.

In addition, we performed XPS measurements of Y_2CF_2 that we kept in a scintillation vial in the glovebox for 1 month. High-resolution scans are shown in the main text (Figure 6). The carbons *1s* spectrum reveals a peak at 279.6 eV, which we attribute to carbidic carbon in Y_2CF_2. We considered other possibilities that the signal could be due to other elements, which have signals at similar binding energies (Os *4d*, Ru *3d*, Sr *3p*, Tb *4p*, and Cl *2s*). We rule out Os, Sr, Tb, and Cl becuase the XPS survey scan (Figure S14) reveals that the most intense peaks for these elements are absent (Os *4f* at 50–55 eV,[7] Sr *3d* and *3s* at 130–135 eV and 357 eV respectively,[8] Tb *4d* at 150 eV,[9] and Cl *2p* at 208 eV[10]). The most intense peak for Ru is the *3d* peak. Therefore, we cannot rule out Ru directly. However, we have no reason to suspect the incorporation of Ru into our sample and its weaker peaks are absent (Ru *4s* at 75 eV, Ru *3p* at 463 eV, and Ru *3s* at 586 eV).[11]

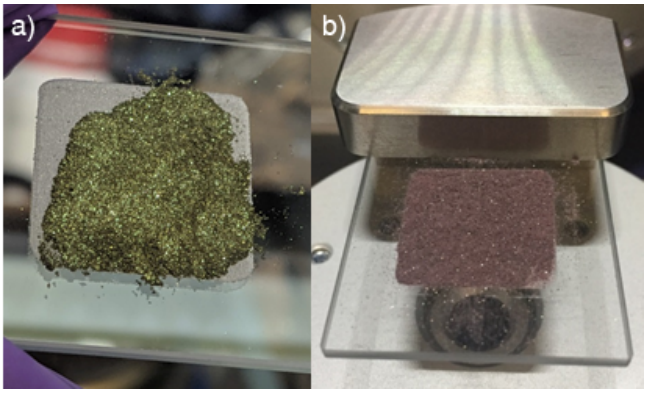

Figure S10: Photographs of a) unoxidized Y_2CF_2 kept in a glovebox and b) oxidized Y_2CF_2 let sit in air for 1 week.

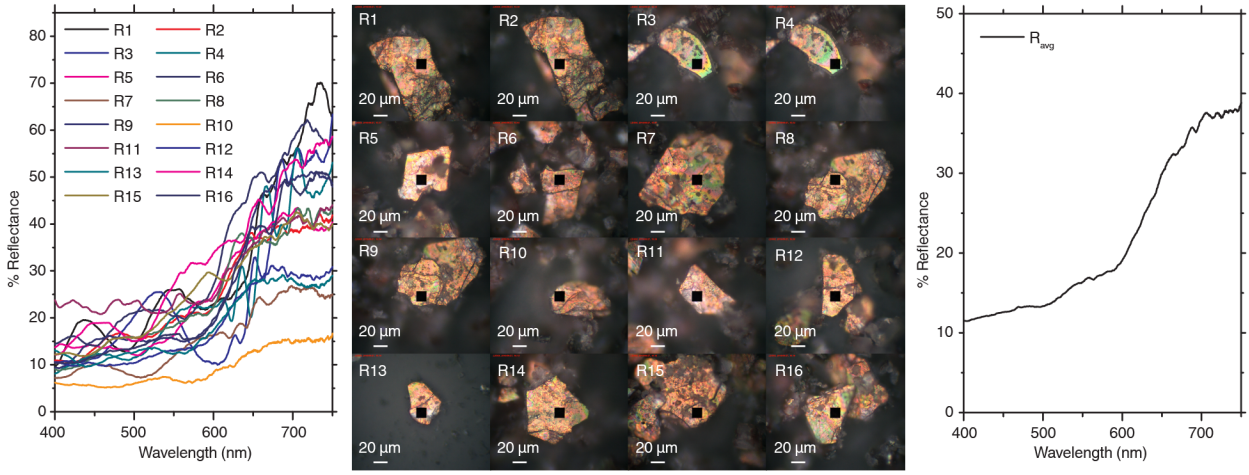

Figure S11: Reflectivity of Y_2CF_2 exposed to air for 1 month and images of the corresponding crystals from which the spectra were acquired. Wavelength-dependent oscillations in the reflectivity spectra and the rainbow-like coloration visible in the images intimates of thin-film effects altering the reflection at the surface. No peak is visible at 540 nm. Instead, on average, shown on the right, the reflectivity decreases at higher energy wavelengths as a fraction of that light is absorbed by the sample. The red powder is shown in the images on the right.

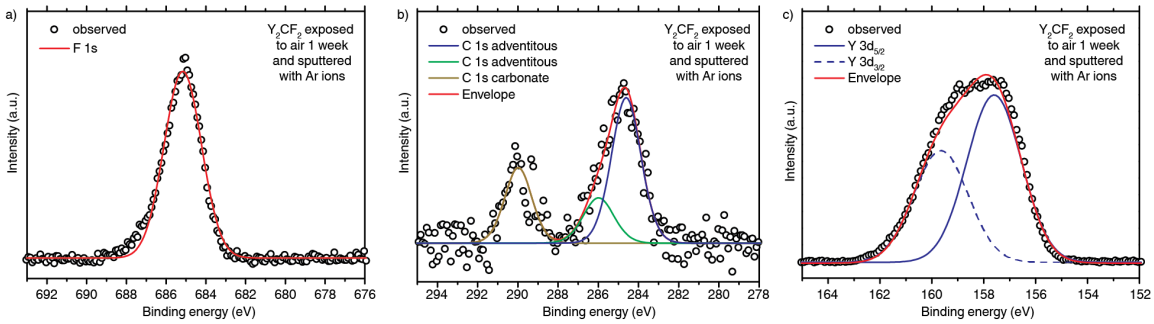

Figure S12: XPS scan of Y_2CF_2 exposed to air for 1 week and then sputtered with Ar-ions for 15 minutes inside of the XPS showing the F *1s*, C *1s*, and Y *3d* spectra. All peaks broadened considerably after sputtering.

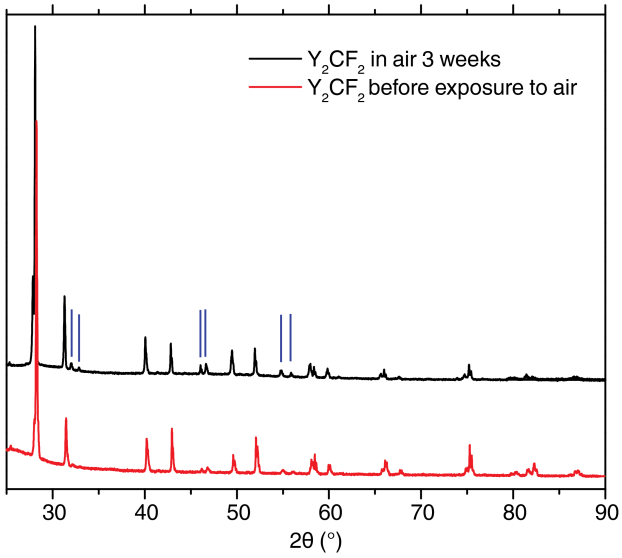

Figure S13: X-ray diffraction patterns collected using the Bragg-Brentano reflection geometry of Y_2CF_2 exposed to air for 3 weeks (black) and the pattern acquired before exposure to air (red). The pattern changes only slightly suggesting that the oxidation process is slow. Marked in blue are peaks from the crystalline phase α-YOF. The intensity of these peaks increases with prolonged exposure to air.

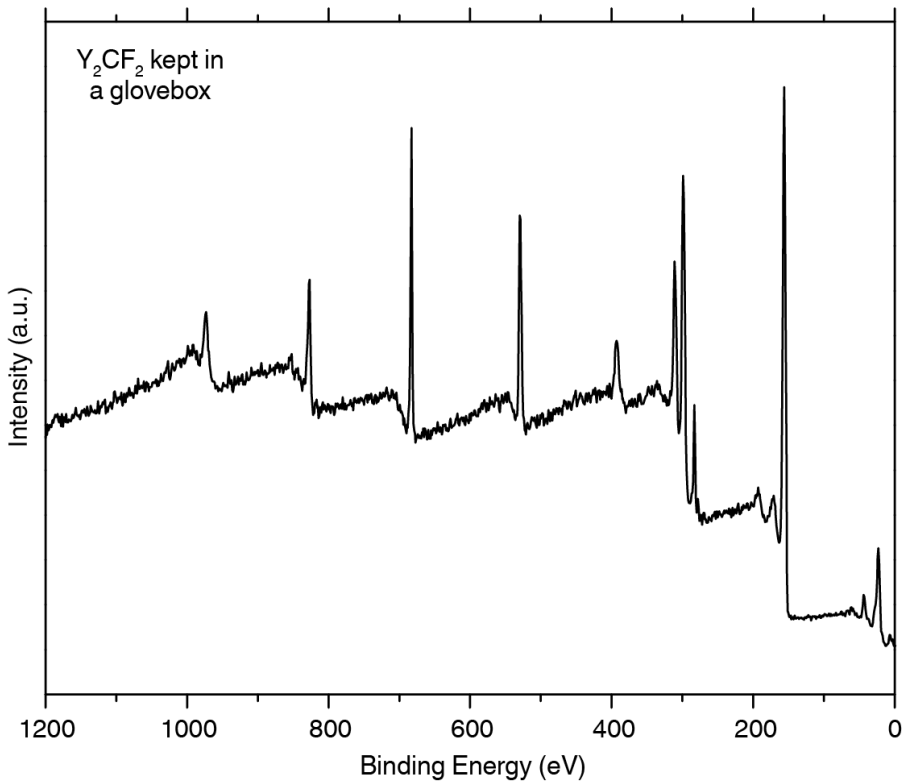

Figure S14: XPS survey scan of Y_2CF_2 kept in a glovebox.

References

(1) Habermann, C.; Daane, A. The preparation and properties of distilled yttrium. *J. Less Common Met.* **1963**, *5*, 134–139.

(2) Savvatimskiy, A. Measurements of the melting point of graphite and the properties of liquid carbon (a review for 1963–2003). *Carbon* **2005**, *43*, 1115–1142.

(3) Brewer, L., et al. *Chemistry and Metallurgy of Miscellaneous Materials: Thermodynamics*; McGraw-Hill New York, 1950; Vol. 19; p 193.

(4) Hwu, S.-J.; Ziebarth, R. P.; von Winbush, S.; Ford, J. E.; Corbett, J. D. Synthesis and structure of double-metal-layered scandium, yttrium, and zirconium chloride carbides and nitrides, M_2Cl_2C and M_2Cl_2N. *Inorg. Chem.* **1986**, *25*, 283–287.

(5) Halim, J.; Cook, K. M.; Naguib, M.; Eklund, P.; Gogotsi, Y.; Rosen, J.; Barsoum, M. W. X-ray photoelectron spectroscopy of select multi-layered transition metal carbides (MXenes). *Appl. Surf. Sci.* **2016**, *362*, 406–417.

(6) Magnuson, M.; Halim, J.; Näslund, L.-Å. Chemical bonding in carbide MXene nanosheets. *J. Electron Spectrosc.* **2018**, *224*, 27–32.

(7) Nyholm, R.; Berndtsson, A.; Martensson, N. Core level binding energies for the elements Hf to Bi (Z= 72–83). *J. Phys. C: Solid State Phys.* **1980**, *13*, L1091.

(8) Vasquez, R. P. SrF_2 by XPS. *Surf. Sci. Spectra* **1992**, *1*, 24–30.

(9) Padalia, B. D.; Gimzewski, J. K.; Affrossman, S.; Lang, W. C.; Watson, L. M.; Fabian, D. J. The reactions of oxygen and water with the rare-earth metals terbium to lutetium studied by x-ray photoelectron spectroscopy. *Surf. Sci.* **1976**, *61*, 468–482.

(10) Vasquez, R. P.; Foote, M. C.; Hunt, B. D. Reaction of nonaqueous halogen solutions with $YBa_2Cu_3O_{7-x}$. *J. Appl. Phys.* **1989**, *66*, 4866–4877.

(11) Nyholm, R.; Martensson, N. Core level binding energies for the elements Zr–Te (Z= 40–52). *J. Phys. C: Solid State Phys.* **1980**, *13*, L279.